^{3}He on preplated graphite

M. C. Gordillo
Departamento de Sistemas Físicos, Químicos y Naturales, Universidad Pablo de Olavide, E-41013 Seville, Spain

J. Boronat
Departament de Física, Universitat Politècnica de Catalunya, Campus Nord B4-B5, E-08034 Barcelona, Spain
(Received 26 July 2016; published 18 October 2016)

By using the diffusion Monte Carlo method, we obtained the full phase diagram of ^{3}He on top of graphite preplated with a solid layer of ^{4}He. All the ^{4}He atoms of the substrate were explicitly considered and allowed to move during the simulation. We found that the ground state is a liquid of density 0.007 ± 0.001 Å^{-2}, in good agreement with available experimental data. This is significantly different from the case of ^{3}He on clean graphite, in which both theory and experiment agree on the existence of a gas-liquid transition at low densities. Upon an increase in ^{3}He density, we predict a first-order phase transition between a dense liquid and a registered $7/12$ phase, the $4/7$ phase being found metastable in our calculations. At larger second-layer densities, a final transition is produced to an incommensurate triangular phase.

DOI: 10.1103/PhysRevB.94.165421

I. INTRODUCTION

Recent heat-capacity studies of ^{3}He on graphite [1–3], both clean and preplated, have reopened the interest on the phase diagram of this quasi-two dimensional (quasi-2D) system. In essence, those results confirm a previous hint about the existence of a stable ^{3}He liquid at very low densities [4] and are the continuation of a wealth of experimental work on this quantum fluid [2,5–12]. On clean graphite, the introduction of corrugation in the theoretical description of the surface [13,14] proved to be the necessary ingredient to produce a good match between those calculations and the experimental results of Sato *et al.* [2] that indicated the existence of a gas-liquid transition at very low densities. When flat substrates were considered, no liquid was found to be stable in most calculations [15–20], but not in all of them [21].

When ^{3}He is adsorbed on ^{4}He-preplated graphite, the experimental data of Ref. [2] shows a linear dependence of the heat capacity versus the second layer density in the range $\rho \sim 0$–0.007 Å^{-2}. This suggests that the ground state of that ^{3}He monolayer is a homogeneous liquid with a density fixed by the upper bound of the interval. For a smaller number of atoms on the same surface, the system is fragmented in drops of 0.007 Å^{-2} with enough empty space between them to produce the average 2D helium concentration we consider. This is different from what happens in the first layer adsorbed directly on graphite [2,13,14] in which there is a gas of ~ 0.006 Å^{-2} in equilibrium with a liquid of ~ 0.014 Å^{-2}. In this second case, what we have are drops of density 0.014 Å^{-2} surrounded by a gas of 0.006 Å^{-2} in the right proportions to produce any density in that range. When ρ is above 0.007 and 0.014 Å^{-2} for the second and first layers, respectively, we have homogeneous liquids covering all the surface.

In this work, we calculate the complete phase diagram of ^{3}He on ^{4}He preplated graphite, including the high density solid region. Given the importance of considering corrugation in the description of the bare substrate, we considered explicitly all the ^{4}He atoms on the first layer, allowing them to move during the simulations. This means that there can be deviations between the actual positions of those atoms and their corresponding crystallographical sites. That produced larger error bars in the statistical sampling than in the case of a flat surface, but it was found to be necessary to reproduce the experimental results, both in the low and high density regimes.

The rest of the paper is organized as follows. In Sec. II, we discuss the quantum Monte Carlo method used for the simulations and account for the interaction models and trial wave functions used as importance sampling. The obtained results and their comparison with experimental data are reported in Sec. III. Finally, Sec. IV comprises the main conclusions of the paper.

II. METHOD

We rely on a microscopic approach to the physical problem of a second layer of ^{3}He atoms adsorbed on ^{4}He-preplated graphite. The Hamiltonian is written as

$$H = -\frac{\hbar^2}{2m_4}\sum_{i=1}^{N_4}\nabla_i^2 - \frac{\hbar^2}{2m_3}\sum_{i=1}^{N_3}\nabla_i^2 + \sum_{i=1}^{N} V_{\rm ext}(\mathbf{r}_i) + \sum_{i<j}^{N} V(r_{ij})\,, \quad (1)$$

where N_3 and N_4 are the number of ^{3}He and ^{4}He atoms ($N = N_3 + N_4$), of masses m_3 and m_4, respectively. $V_{\rm ext}(\mathbf{r})$ is the total interaction of each helium atom at position $\mathbf{r}$ with all the carbon atoms in the graphite substrate. This term is made up of a sum of individual C-He interactions, each of them modeled by the anisotropic Carlos-Cole potential [22,23], even though no influence of the C-He anisotropy is expected in the behavior of the second layer, as has been already proved for a second layer of ^{4}He on the same substrate [23]. As in previous works, the substrate structure was modeled by a stack of honeycomb 2D lattices separated by 3.35 Å in the typical A-B-A-B graphite disposition [24–26]. $V(r)$ is the standard Aziz potential for the helium-helium interaction [27] of two atoms separated by a distance r.

 ©2016 American Physical Society

We considered unpolarized ^{3}He, i.e., $N_\uparrow = N_\downarrow = N_3/2$. To solve the N-body Schrödinger equation corresponding to the Hamiltonian of Eq. (1), we used the fixed-node diffusion Monte Carlo (FN-DMC) method. This stochastic technique solves the Schrödinger equation in imaginary time, providing the exact energy for the ground state of a Bose system and an upper bound for a Fermi one [28]. This means that our results are only strictly valid at 0 K. Our system consists of a mixture of bosons (^{4}He) and fermions (^{3}He), and thus we get an upper bound to the exact energy whose quality depends on the proximity of the nodal surface of the trial wave function (used for importance sampling) to the (unknown) exact one. Our trial wave function was

$$\Phi(\mathbf{r}_1,\mathbf{r}_2,\ldots,\mathbf{r}_N) = \Psi_3(\mathbf{r}_1,\mathbf{r}_2,\ldots,\mathbf{r}_{N_3}) \times \Psi_4(\mathbf{r}_{N_3+1},\mathbf{r}_{N_3+2},\ldots,\mathbf{r}_N) \quad (2)$$

with $\mathbf{r}_1,\mathbf{r}_2,\ldots,\mathbf{r}_{N_3}$ the coordinates of the N_3 ^{3}He atoms in the second layer, and $\mathbf{r}_{N_3+1},\mathbf{r}_{N_3+2},\ldots,\mathbf{r}_N$ the ones for the N_4 remaining ^{4}He atoms in the first layer, in direct contact with graphite. This means that, by construction, the two helium layers are separated from each other, what we think a reasonable approximation in light of the available experimental results. Following Ref. [14], we defined

$$\Psi_3(\mathbf{r}_1,\mathbf{r}_2,\ldots,\mathbf{r}_{N_3}) = D^\uparrow D^\downarrow \prod_i^{N_3} u_3(\mathbf{r}_i) \times \prod_{i<j}^{N_3} \exp\left[-\frac{1}{2}\left(\frac{b_3}{r_{ij}}\right)^5\right], \quad (3)$$

where $D^\uparrow$ and $D^\downarrow$ are the Slater determinants of the two-dimensional system defined by our simulation cell that depend on the coordinates of the spin-up and spin-down ^{3}He fermions. The one-body function $u_3(\mathbf{r})$ is the numerical solution of the Schrödinger equation that describes a single ^{3}He atom on top of a triangular lattice formed by ^{4}He atoms located in the crystallographic positions $(x_{\rm site}, y_{\rm site})$ corresponding to an incommensurate triangular phase. To solve this equation, we used the same technique as in Ref. [14] and neglected the influence of the underlying graphite structure. In the present work, we used two triangular ^{4}He lattices at different densities: 0.112 Å^{-2} (corresponding to a separation of 3.2 Å) and 0.12 Å^{-2} (with a He-He lattice constant of 3.1 Å). The first density corresponds to the ^{4}He promotion to the second layer [11,29], while the latter is the upper experimental limit given in Ref. [2], a limit slightly larger than the one given in Ref. [11] ($\rho \sim 0.116$ Å^{-2}). The parameter b_3 in Eq. (3) is variationally optimized; its value is set to $b_3 = 2.96$ Å, as in Refs. [14,19]. The coordinates in the Slater determinants were corrected by backflow terms in the standard way,

$$\tilde{x}_i = x_i + \lambda \sum_{j\neq i} \exp[-(r_{ij}-r_b)^2/\omega^2](x_i - x_j) \quad (4)$$

$$\tilde{y}_i = y_i + \lambda \sum_{j\neq i} \exp[-(r_{ij}-r_b)^2/\omega^2](y_i - y_j). \quad (5)$$

The optimal values for the parameters in the backflow term were those of the bulk three-dimensional system [30], i.e., $\lambda = 0.35$, $\omega = 1.38$ Å, and $r_b = 1.89$ Å, since they were proved to give lower energies [14] that those corresponding to a pure 2D system [19].

The part of the trial wave function corresponding to the first ^{4}He layer is taken as

$$\Psi_4(\mathbf{r}_{N_3+1},\mathbf{r}_{N_3+2},\ldots,\mathbf{r}_N) = \prod_i^{N_4} u_4(\mathbf{r}_i) \prod_{i<j}^{N_4} \exp\left[-\frac{1}{2}\left(\frac{b_4}{r_{ij}}\right)^5\right] \times \prod_i^{N_4} \exp\{-a_4[(x_i - x_{\rm site})^2 + (y_i - y_{\rm site})^2]\}. \quad (6)$$

The last (Nosanov) term in the equation pines the atoms around their crystallographic positions. The free parameters in Ψ_4 are: $b_4 = 3.07$ Å (as in Refs. [24,29]), and a_4 has the same value as that in a previous study of the second layer of ^{4}He on ^{4}He (0.55 Å^{-2}) [29]. As before, $u_4(\mathbf{r}_i)$ is the numerical solution of the one-body Schrödinger equation for one ^{4}He atom on top of graphite.

Equation (2) defines adequately the ^{3}He layer when it is a liquid or a gas. If this is not so, we have to introduce a Nosanov term to confine the ^{3}He atoms,

$$\prod_i \exp\{-a_3[(x_i - x_{\rm site})^2 + (y_i - y_{\rm site})^2]\}\,, \quad (7)$$

in which we used the same a_3 parameter for all the solid phases and densities ($a_3 = 0.24$ Å^{-2}). [14] We checked that neither an increase or a decrease of up to 50% in a_3 varies the stability ranges of the solids described. The trial wave function (2) is factorized in a term depending only on the ^{3}He coordinates and another only on the ^{4}He ones. Simulations including a Jastrow term relating atoms in both layers produced no significant change in the obtained results.

III. RESULTS

In Fig. 1 we show the FN-DMC results for the energy per ^{3}He atom as a function of the second-layer density. The upper (lower) curve corresponds to a fixed first-layer density of 0.112 (0.12) Å^{-2}. We chose those densities as lower and upper limits to the magnitude at hand and used these two set of simulations to test the effect of a possible compression of the ^{4}He solid structure upon an increase of the number of ^{3}He atoms on top of it. The curves displayed are third-order degree polynomials obtained by least-squares fitting to the shown data.

From those fits, we can state that the energy per ^{3}He atom on ^{4}He-preplated graphite in the infinite dilution limit, E_0, is -24.45 ± 0.04 K in the first case and -24.74 ± 0.07 K for the denser preplating, values much smaller in absolute value than the same magnitude for ^{3}He on bare graphite, -135.771 ± 0.001 K [14]. In both cases, we used a simulation cell that comprised 14×8 incommensurate triangular lattice cells. Those rectangular unit cells contain two ^{4}He atoms and have a surface $d_{\rm He} \times \sqrt{3} d_{\rm He}$, $d_{\rm He}$ being the distance between two atoms in the first layer. This means that for the upper curve the simulation cell was 44.8×44.34 Å^2, and for the lower one, 43.4×42.95 Å^2. In both cases, that means 224 ^{4}He atoms on

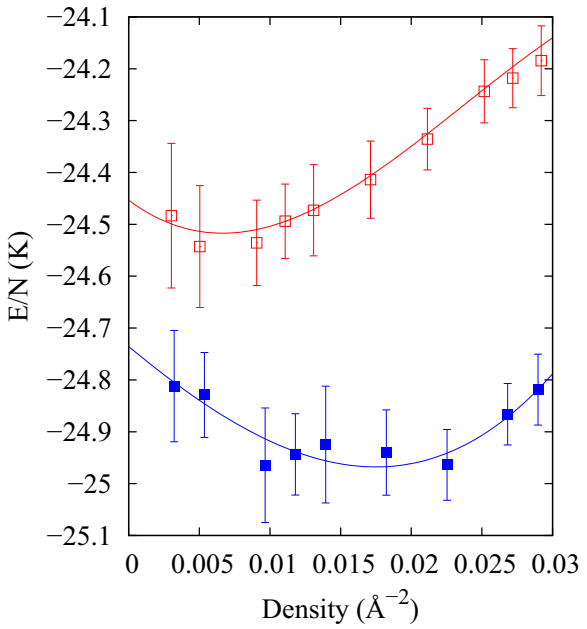

FIG. 1. Energy per ^{3}He atom (E/N) on the second layer of ^{3}He on graphite as a function of the second-layer density. Upper curve, underlying ^{4}He density 0.112 Å^{-2}; lower curve, first layer density 0.12 Å^{-2}). The curves are third-order polynomial fits to the data displayed.

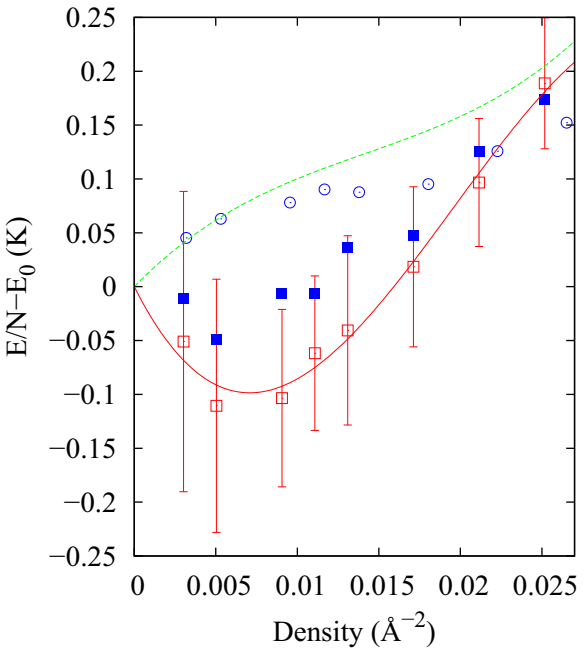

FIG. 2. Same as in the previous figure, but after subtracting the infinite dilution limit energies (E_0's). Lower open squares with error bars, our simulation results for ^{3}He on top of an active first ^{4}He layer; upper full squares without error bars, same but for a fixed ^{4}He layer with atoms located in their crystallographic positions; open circles, results for a second ^{3}He layer on a first averaged over potential. The lower line corresponds to the same third-order polynomial fit of the previous figure, and the upper one, to the pure 2D result of Ref. [19].

the lower layer and enough ^{3}He atoms to produce the densities shown. This means up to 102 ^{3}He atoms in the case of the second-layer liquids discussed below. In all the simulations, standard finite-size corrections to the fermionic wave function were applied. As indicated in the preceding section, all the ^{4}He atoms on the first layer were allowed to move during the simulations, i.e., we solve the full Hamiltonian (1).

Our results, reported in Fig. 1, show the second layer is a liquid, since in both cases we have self-bound structures of densities 0.007 ± 0.001 Å^{-2} (upper curve) and 0.017 ± 0.001 Å^{-2} (lower one). Those values were obtained from the fits displayed. Different from the first layer on bare graphite structure, no gas-liquid transition was found. To our knowledge, the only experimental set of available data to compare our results to are those of Ref. [2]. As indicated above, at very low densities, the experimental heat capacity depends linearly on the second layer density in the range 0–0.007 Å^{-2}. This would indicate a phase separation between a clean surface and a homogeneous liquid of 0.007 Å^{-2}. This is exactly what can be deduced from the upper curve of Fig. 1. From that, we can conclude that a model with a preplated density of 0.112 Å^{-2} is a good description of the experimental setup.

Our results are different from the results of a previous theoretical calculation on this same system [13]. In that work, the authors found a gas-liquid transition of the same type as the one for the first layer on bare graphite. To explain that discrepancy, we use the results displayed in Fig. 2. There, the lower set of data is the one in the previous figure after having subtracted the energy in the infinity dilution limit, E_0. On the other hand, the open circles correspond to a calculation in which the effect of the first ^{4}He layer and the graphite surface below it have been described by a laterally z-averaged potential, something similar to the description made in Ref. [13]. In this flat case, $E_0 = -26.313 \pm 0.001$ K. Even though the results in Ref. [13] are not exactly the same as the ones in Fig. 2 since the helium-helium potentials are slightly different, both sets of data look pretty similar to each other. At the same time, both of them are noticeably different from the simulations made with the full Hamiltonian (1). The error bars of those results are of the size of the symbols and not displayed for simplicity.

The missing ingredient is the corrugation of the ^{4}He substrate, as in the bare graphite case. To check that, we repeated our calculations but without allowing the movement of the ^{4}He atoms in the first layer. What we see is that those results are within the (rather large) error bars of those corresponding to the full ^{4}He-moving calculation and present a minimum at approximately the same density. In our opinion, this indicates that the introduction of a ^{3}He effective mass, used in the Ref. [13] calculations, is not enough to compensate for the use of a z-averaged potential. The error bars of these last results are comparable, though somewhat smaller than the ones for the full calculation, and again were not displayed for simplicity.

Figure 3 shows the high density end of the $T = 0$ isotherm for a 0.112 Å^{-2} underlying density. There, we have displayed the energies per ^{3}He atom corresponding to a liquid phase (full squares), incommensurate triangular solid (open squares), and two standard commensurate structures on second-layer-

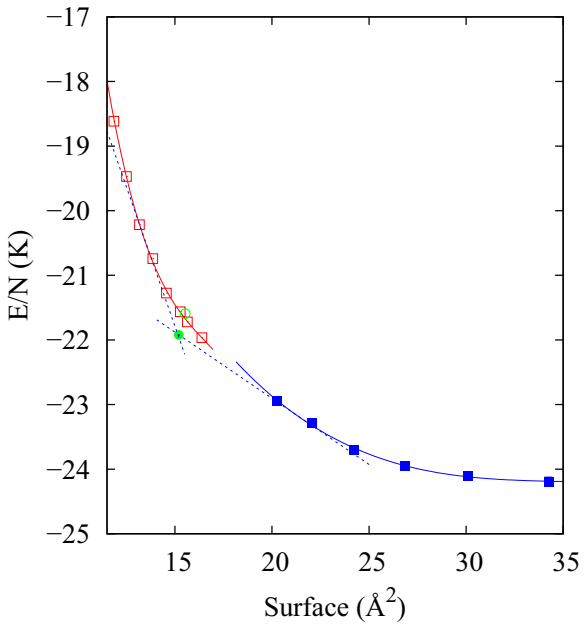

FIG. 3. Energy per ^{3}He atom (E/N) on the second layer of helium on graphite on top of a 0.112 Å^{-2} ^{4}He layer, as a function of the inverse of the second layer density. Solid squares, liquid phase; open squares, triangular incommensurate structure; full circle, 7/12 phase; open circle, 4/7 commensurate solid. Solid lines are mere guides to the eye. Dotted lines correspond to Maxwell constructions between the different stable phases.

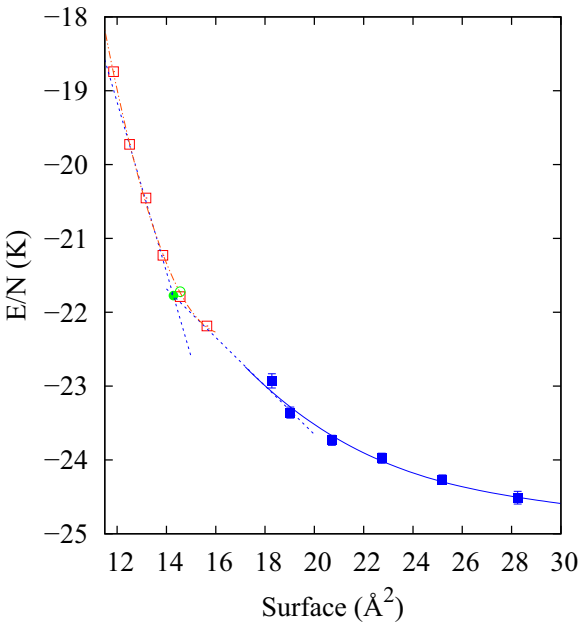

FIG. 4. Same as in the previous figure, but for a ^{4}He density of 0.12 Å^{-2}.

helium structures: 4/7 (open circle), and 7/12 (full circle). By a simple inspection, we can see that there is practically no difference between the energies of the 4/7 lattice, of density 0.064 Å^{-2}, and that of an incommensurate triangular structure of the same density. In addition, the energy per particle of a 7/12 structure is lower than both the one corresponding to the 4/7 commensurate solid and that of the incommensurate arrangement of equal density (0.066 Å^{-2}). This means that we can draw a double-tangent Maxwell construction line that starts in a liquid of density 0.047 ± 0.002 Å^{-2} and ends in the energy corresponding to that 7/12 structure, i.e., those phases are in equilibrium with each other. When the density increases further, another Maxwell construction shows that the 7/12 solid is in equilibrium with an incommensurate triangular one of density 0.072 ± 0.004 Å^{-2} that is probably stable up to the third layer promotion.

In the same way as before, to check for the influence of the first layer density on the phase diagram of the second layer, we performed another series of calculations for a ^{4}He density of 0.12 Å^{-2}. The results are displayed in Fig. 4, where the symbols and lines have the same meaning as in the previous figure. The main differences are the densities at which the different transitions are produced: The liquid is now stable up to 0.054 ± 0.002 Å^{-2}, and it is in equilibrium with a 7/12 commensurate solid of 0.070 Å^{-2} that undergoes a first-order phase transition to a triangular solid of $\rho = 0.074 \pm 0.002$ Å^{-2}. If, as suggested in Ref. [11], the density of the first ^{4}He layer in a real setup is between those considered here, one would expect density limits for the stable phases in between those reported for the two sets of simulation results.

With that in mind, we can say that our results compare favorably with the available experimental data. In particular, a solid is found for second layer densities larger than [10] 0.072 Å^{-2}, a density which is well within the error bars of our results in both series of simulation data. This would correspond to the lower stability limit of the triangular phase. In addition, magnetization [31] and heat-capacity [9] measurements on a double ^{3}He layer give a solid-solid transition region similar to the one that we see from a commensurate structure to the lower density for which the incommensurate phase is stable (total density in the range 0.179 and 0.185 Å^{-2}). However, even though those data are close to our results, they are not directly comparable to them, since it is well known that the density of the first layer of the system ^{3}He/^{3}He/graphite is ∼5% smaller than the ^{3}He/^{4}He/graphite one [32]. Finally, the experimental upper second layer density for a liquid in equilibrium with the commensurate phase (7/12 in our case, but 4/7 in virtually all the previous literature) is [11] 0.058 ± 0.005 Å^{-2}. This is comparable to our 0.12 Å^{-2} result, which would support a compression of the first layer upon population of the first one.

IV. DISCUSSION

In this work, we have calculated the complete phase diagram of a ^{3}He layer on top of ^{4}He-preplated graphite at 0 K. The main difference with previous theoretical approaches is that we have considered a full three-dimensional system and allowed the ^{4}He atoms of the first layer to move. This produces a low-density phase diagram that is appreciably different from that for a flat [19] or z-averaged [13] substrate. This result is not surprising, since corrugation [33,34] and disorder [29,35] have been found to be important in double

layer ^{4}He simulations. However, the fact that our results are comparable to the experimental data of Ref. [2] confirms the quality of our approximations. The rest of the phase diagram is pretty close to the experimental data, with phases and stability ranges that are in good agreement each other.

However, there is a significant difference. The commensurate phase that we found to be in equilibrium with the dense liquid and the triangular solid is a 7/12, not the 4/7, as it appears in the literature. To try to understand this, we should have in mind that the difference in densities between those two phases is very small (∼3%, expressed as density of the second layer only). This means that it could be experimentally difficult to distinguish them, especially taking into account that the first layer densities can vary. On the other hand, our Hamiltonian does not include any ferromagnetic or antiferromagnetic spin-spin interaction, something that could be important and eventually change the relative stability of the 4/7 and 7/12 phases.

ACKNOWLEDGMENTS

We thank H. Godfrin and H. Fukuyama for illuminating discussions. We acknowledge partial financial support from the Junta de Andalucía group PAI-205 and MINECO (Spain) Grants No. FIS2014-56257-C2-2-P and No. FIS2014-56257-C2-1-P.

[1] D. Sato, T. Tsuji, S. Takayoshi, K. Obata, T. Matsui, and H. Fukuyama, J. Low Temp. Phys. **158**, 201 (2010).
[2] D. Sato, K. Naruse, T. Matsui, and H. Fukuyama, Phys. Rev. Lett. **109**, 235306 (2012).
[3] Ashley G. Smart, Phys. Today **66**(1), 16 (2013).
[4] B. K. Bhattacharyya and F. M. Gasparini, Phys. Rev. B **31**, 2719 (1985).
[5] D. S. Greywall, Phys. Rev. B **41**, 1842 (1990).
[6] D. S. Greywall and P. A. Busch, Phys. Rev. Lett. **65**, 64 (1990).
[7] H. Godfrin, R. E. Rapp, K. D. Morhard, J. Bossy, and C. Bauerle, Phys. Rev. B **49**, 12377 (1994).
[8] K. D. Morhard, C. Baüerle, J. Bossy, Y. Bunkov, S. N. Fisher, and H. Godfrin, Phys. Rev. B **53**, 2658 (1996).
[9] M. Siqueira, J. Nyeki, B. Cowan, and J. Saunders, Phys. Rev. Lett. **76**, 1884 (1996).
[10] C. Bäuerle, Y. Bunkov, A. S. Chen, S. N. Fisher, and H. Godfrin, J. Low Temp. Phys. **110**, 333 (1998).
[11] M. Roger, C. Bauerle, H. Godfrin, L. Pricoupenko, and J. Treiner, J. Low Temp. Phys. **112**, 451 (1998).
[12] E. Collin, S. Triqueneaux, R. Harakaly, M. Roger, C. Bäuerle, Y. M. Bunkov, and H. Godfrin, Phys. Rev. Lett. **86**, 2447 (2001).
[13] M. Ruggeri, E. Vitali, D. E. Galli, M. Boninsegni, and S. Moroni, Phys. Rev. B **93**, 104102 (2016).
[14] M. C. Gordillo and J. Boronat, Phys. Rev. Lett. **116**, 145301 (2016).
[15] A. D. Novaco and C. E. Campbell, Phys. Rev. B **11**, 2525 (1975).
[16] M. D. Miller and L. H. Nosanov, J. Low Temp. Phys. **32**, 145 (1978).
[17] C. Um, J. Kahng, Y. Kim, T. F. George, and L. N. Pandey, J. Low Temp. Phys. **107**, 283 (1997).
[18] B. Krishnamachari and G. V. Chester, Phys. Rev. B **59**, 8852 (1999).
[19] V. Grau, J. Boronat, and J. Casulleras, Phys. Rev. Lett. **89**, 045301 (2002).
[20] M. Ruggeri, S. Moroni, and M. Boninsegni, Phys. Rev. Lett. **111**, 045303 (2013).
[21] B. Brami, F. Joly, and C. Lhuillier, J. Low Temp. Phys. **94**, 63 (1994).
[22] W. E. Carlos and M. W. Cole, Surf. Sci. **91**, 339 (1980).
[23] M. C. Gordillo and J. Boronat, J. Low Temp. Phys. **171**, 606 (2013).
[24] M. C. Gordillo and J. Boronat, Phys. Rev. Lett. **102**, 085303 (2009).
[25] M. C. Gordillo, Phys. Rev. B **89**, 155401 (2014).
[26] M. C. Gordillo, C. Cazorla, and J. Boronat, Phys. Rev. B **83**, 121406(R) (2011).
[27] R. A. Aziz, F. R. W. McCourt, and C. C. K. Wong, Mol. Phys. **61**, 1487 (1987).
[28] B. L. Hammond, W. A. Lester, Jr., and P. J. Reynolds, *Monte Carlo Methods in Ab Initio Quantum Chemistry* (World Scientific, Singapore, 1994).
[29] M. C. Gordillo and J. Boronat, Phys. Rev. B **85**, 195457 (2012).
[30] J. Casulleras and J. Boronat, Phys. Rev. Lett. **84**, 3121 (2000).
[31] C. Bäuerle, Ph.D. thesis, Université J. Fourier, CRTBT-CNRS, Grenoble, 1996.
[32] H. Fukuyama, J. Phys. Soc. Jpn. **77**, 111013 (2008).
[33] M. Pierce and E. Manousakis, Phys. Rev. Lett. **81**, 156 (1998).
[34] M. Pierce and E. Manousakis, Phys. Rev. B **59**, 3802 (1999).
[35] P. Corboz, M. Boninsegni, L. Pollet, and M. Troyer, Phys. Rev. B **78**, 245414 (2008).